Letter

Long-distance chronometric leveling with a portable optical clock

J. Grotti,[1,†] I. Nosske,[1,†] S.B. Koller,[1] S. Herbers,[1] H. Denker,[2] L. Timmen,[2] G. Vishnyakova,[3] G. Grosche,[1] T. Waterholter,[1] A. Kuhl,[1] S. Koke,[1] E. Benkler,[1] M. Giunta,[3,4] L. Maisenbacher,[3] A. Matveev,[3] S. Dörscher,[1] R. Schwarz,[1] A. Al-Masoudi,[1] T.W. Hänsch,[3] Th. Udem,[3] R. Holzwarth,[3,4] and C. Lisdat[1,*]

[1] *Physikalisch-Technische Bundesanstalt, Bundesallee 100, 38116 Braunschweig, Germany*

[2] *Institut für Erdmessung, Leibniz Universität Hannover (LUH), Schneiderberg 50, 30167 Hannover, Germany*

[3] *Max-Planck-Institut für Quantenoptik, Hans-Kopfermann-Straße 1, 85748 Garching, Germany*

[4] *Menlo Systems GmbH, Bunsenstraße 5, 82152 Martinsried, Germany*

(Received 21 September 2023; revised 29 April 2024; accepted 1 May 2024; published 3 June 2024)

We have measured the geopotential difference between two locations separated by 457 km by comparison of two optical lattice clocks via an interferometric fiber link, utilizing the gravitational redshift of the clock transition frequency. The ^{87}Sr clocks have been compared side-by-side before and after one of the clocks was moved to the remote location. The chronometrically measured geopotential difference of 3918.1(2.6) $m^2\ s^{-2}$ agrees with an independent geodetic determination of 3915.88(0.30) $m^2\ s^{-2}$. The uncertainty of the chronometric geopotential difference is equivalent to an uncertainty of 27 cm in height.

DOI: 10.1103/PhysRevApplied.21.L061001

According to general relativity, clocks located in gravity potentials that differ by ΔU experience a tick rate difference that is given in relative units by $\Delta U/c^2$ in the first (Newtonian) order, which is known as the gravitational redshift. While this is a small effect, modern optical atomic clocks with their outstanding fractional uncertainty of approximately 10^{-18} [1–4] can resolve a potential difference corresponding to a height difference of $\Delta h \sim 1$ cm close to the geoid, where $\Delta h = \Delta U/g$ for a homogeneous gravitational acceleration g. Furthermore, the frequency of two atomic clocks can be compared via an interferometric fiber link (IFL), which supports sub-10^{-19} accuracy over hundreds of kilometers [5–10]. Hence, determination of gravitational redshift differences with clocks can be utilized in geodesy to revolutionize geopotential and physical height determination capabilities. This method is known as "chronometric leveling" [11–13]. Experiments in this context have been conducted for short [14–19] and long [6,20,21] distances.

Physical heights relate directly to the geopotential (a physical quantity), in contrast to the purely geometrically defined ellipsoidal heights (distance of a point from a given reference ellipsoid) from global navigation satellite system (GNSS) measurements [22]. The most widely known geodetic technique to derive physical heights is geometric leveling (also known as spirit leveling) in combination with local gravity measurements. However, this method becomes fairly labor-intensive for distances of hundreds of kilometers and is prone to the accumulation of errors, which may reach several decimeters over a 1000-km distance. Alternatively, absolute geopotential values with uncertainties at the centimeter level can be obtained using the "GNSS/geoid approach" [23]. It combines ellipsoidal heights from GNSS with an accurate gravity field model (geoid) with high spatial resolution of a few kilometers. The latter is obtained by refining satellite gravity field models with terrestrial gravity measurements and terrain data. Compared with these two established geodetic methods for measuring geopotential differences, the main advantage of chronometric leveling lies in its ability to directly measure potential differences with mostly distance-independent uncertainty.

Previously, extremely small redshifts have been resolved with optical clocks [18,19] by differential observations in a single apparatus. Long-distance geodetic measurements require independent clocks, however. While stationary optical clocks have been compared over long distances [6,20], chronometric leveling requires an additional side-by-side comparison to establish the frequency ratio of the clock apparatuses themselves, i.e., to measure any potential frequency shifts other than the gravitational

*Corresponding author: christian.lisdat@ptb.de

†J.G. and I.N. contributed equally to this work.

Published by the American Physical Society under the terms of the Creative Commons Attribution 4.0 International license. Further distribution of this work must maintain attribution to the author(s) and the published article's title, journal citation, and DOI.

redshift. Hence, at least one of the clocks needs to be transported. Chronometric leveling with a transportable optical clock has been realized with a ^{87}Sr lattice clock [24] between Modane (France) and Torino (Italy), albeit with a moderate fractional frequency uncertainty of 1.9×10^{-15} [21]. Today, several groups operate transportable optical clocks [16,17,25–31]. In a local-area height measurement, an accuracy of 4 cm has been demonstrated [15].

In this work, we demonstrate long-distance chronometric leveling with two optical clocks over a distance of several hundred kilometers with a frequency uncertainty at the low 10^{-17} level (corresponding to a height resolution of a few decimeters). The two connected sites are the Physikalisch-Technische Bundesanstalt (PTB) at Braunschweig, Germany and the Max-Planck Institute of Quantum Optics (MPQ) at Garching, Germany that are 457 km (linear distance) apart and have a height difference of 400 m. They are connected via a 940-km-long IFL (see Fig. 1). PTB's transportable ^{87}Sr lattice clock Sr2 [24] in its air-conditioned car trailer is compared against the stationary ^{87}Sr lattice clock Sr1 [32,33] before, during, and after its stay at MPQ. The local clock comparisons at PTB ensure that the frequency ratio between colocated clocks remains unaffected by the transport and is known. Only then a frequency shift observed at the remote site can be attributed to the gravitational redshift. To verify our chronometric leveling result, we compare it with the result of the GNSS/geoid approach and find good agreement.

Our data are recorded and analyzed as follows. All beat notes between the different lasers are counted with synchronized, dead-time-free counters in phase-averaging (Λ) mode and with an averaging time of 1 s [35,36]. Valid counter data, as determined from auxiliary clock monitoring data, are used to calculate the difference of the measured clock transition frequencies $\Delta\nu^{\mathrm{clock}} = \nu_{\mathrm{Sr2}} - \nu_{\mathrm{Sr1}}$ in one-second intervals. The arithmetic mean of $\Delta\nu^{\mathrm{clock}}$ on each day is denoted by $\Delta\nu^{\mathrm{clock}}_{\mathrm{day}}$.

For the two local campaigns at PTB, we define the daily average clock offset $\Delta\nu^{\mathrm{loc}}_{\mathrm{day}}$ by

$$\Delta\nu^{\mathrm{loc}}_{\mathrm{day}} = \Delta\nu^{\mathrm{clock}}_{\mathrm{day}} + \mathrm{cor}^{\mathrm{Sr2}}_{\mathrm{day}} - \mathrm{cor}^{\mathrm{Sr1}}_{\mathrm{day}} - \Delta\nu^{\mathrm{grav}}_{\mathrm{day}}, \qquad (1)$$

where $\mathrm{cor}^{\mathrm{Sr1}}_{\mathrm{day}}$ and $\mathrm{cor}^{\mathrm{Sr2}}_{\mathrm{day}}$ are the frequency corrections of the respective clocks due to known atomic frequency shifts for a given day of measurement. The gravitational redshift difference is given by $\Delta\nu^{\mathrm{grav}}_{\mathrm{day}} = (\nu_0\, g_{\mathrm{PTB}}/c^2)\, \Delta h_{\mathrm{day}}$, with the clock transition frequency $\nu_0 \approx 429.228$ THz, the speed of light c, the local gravity acceleration $g_{\mathrm{PTB}} \approx 9.813$ m s^{-2}, and the height difference between the two clocks $\Delta h_{\mathrm{day}} = h_{\mathrm{Sr2,day}} - h_{\mathrm{Sr1}}$. The height $h_{\mathrm{Sr2,day}}$ is constant within each local campaign at PTB, but differs slightly between both campaigns, as the transportable clock trailer was installed at slightly different heights. For the local clock comparisons before and after the transport to MPQ, the height difference Δh_{day} of the clocks' atomic clouds is measured by geometric leveling to be $-104(5)$ and $-166(11)$ mm, respectively.

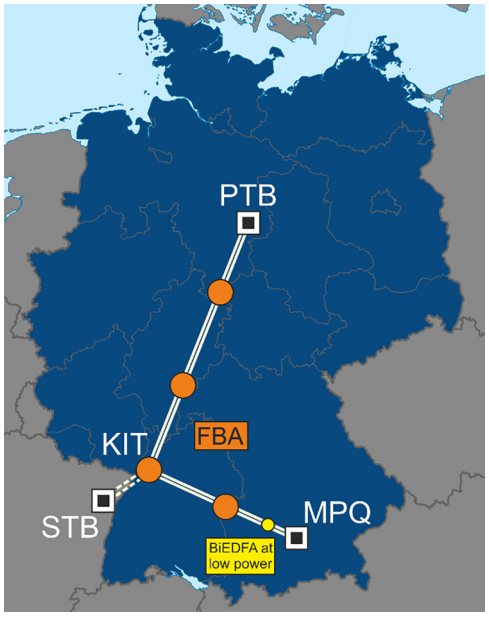


FIG. 1. The 940-km-long IFL between PTB and MPQ, shown on a map of Germany (in blue). Due to attenuation of the link laser light, four fiber Brillouin amplifiers (FBAs) [34] and one bidirectional erbium-doped fiber amplifier (BiEDFA) have been installed along its path. At Karlsruhe Institute of Technology (KIT), the IFL from PTB branches to MPQ and Strasbourg (STB).

The uncertainty $u(\Delta\nu^{\mathrm{loc}}_{\mathrm{day}})$ of the daily data $\Delta\nu^{\mathrm{loc}}_{\mathrm{day}}$ is calculated by summing the uncertainties of the individual terms of Eq. (1) in quadrature. The statistical uncertainty contribution to $\Delta\nu^{\mathrm{clock}}_{\mathrm{day}}$ is estimated from the Allan deviation of the daily measurement extrapolated to the measurement duration. The Allan deviation of the concatenated data set of all local measurements is shown in Fig. 2. The uncertainties of $\mathrm{cor}^{\mathrm{Sr1}}_{\mathrm{day}}$ and $\mathrm{cor}^{\mathrm{Sr2}}_{\mathrm{day}}$ are the systematic uncertainties of the clocks Sr1 and Sr2. Combined, they contribute about 2×10^{-17} and 4×10^{-17} in fractional units of ν_0 to the daily averages of the first and second local comparison campaigns, respectively. In comparison with Ref. [24], the uncertainty of Sr2 is reduced owing to an extended investigation of the cold-collision shift and a combined evaluation of the lattice light shifts of different orders, using the model from Ref. [37]. In both cases, the main reduction of uncertainty is caused by a lower statistical uncertainty of the underlying data sets compared with Ref. [24]. The individual systematic uncertainty contributions of both clocks are listed in Table I. Details are discussed in the Supplemental Material [38] and references therein [24,37,39–52].

We compute the local clock offset $\overline{\Delta\nu}_{\mathrm{loc}}$ as the average over all local measurement days $\Delta\nu^{\mathrm{loc}}_{\mathrm{day}}$ with weights

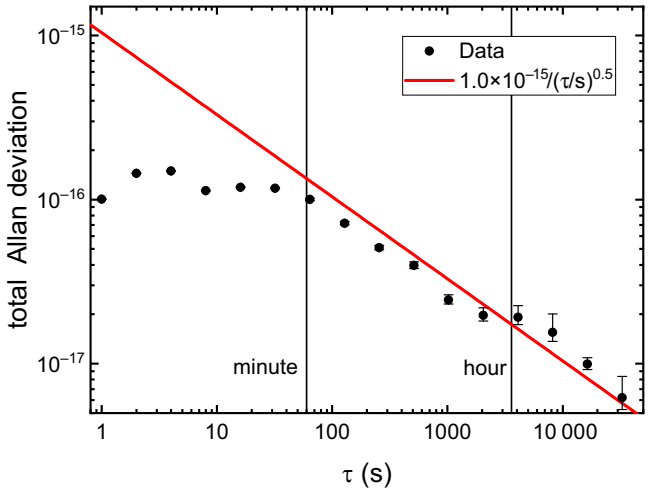


FIG. 2. Total Allan deviation of the concatenated data of the two local clock comparisons as a function of the averaging time τ. The red line indicates the instability and is a $\propto \tau^{-1/2}$ fit to points with $\tau > 100$ s.

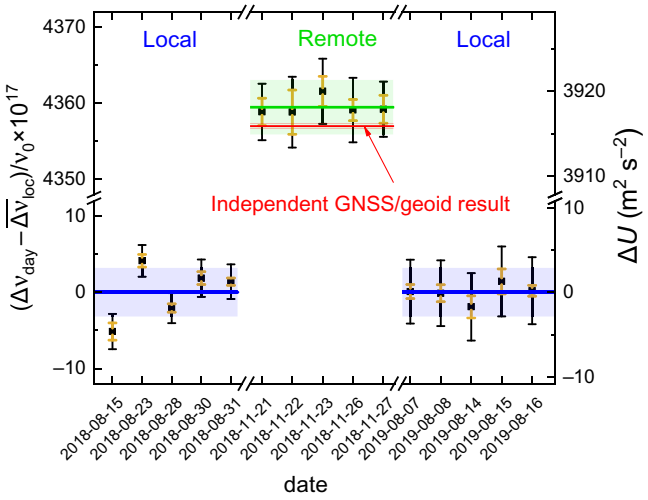


FIG. 3. Daily frequency differences between the transportable clock (Sr2) and the stationary clock (Sr1) during the local and remote clock comparisons, corrected for the measured local clock offset $\overline{\Delta\nu}_{loc}/\nu_0 = 50 \times 10^{-18}$. The plotted data include the clocks' frequency corrections, as well as corrections according to the small geopotential differences during the local measurements. The blue (green) line and shaded areas represent the mean value and uncertainty of the local (remote) clock comparison. The yellow error bars represent daily statistical uncertainties; black error bars show the daily total uncertainties. The red line represents the geodetic result obtained by the combination of GNSS data and geoid modeling [23].

$1/u(\Delta\nu_{day}^{loc})^2$. In order to account for the increased scatter of the daily clock comparison data during the first local campaign, we multiply its daily uncertainties by the data set's Birge ratio [53], which is about 1.7. The uncertainty $u(\overline{\Delta\nu}_{loc})$ is determined taking into account correlations of systematic clock corrections between the different daily measurements [39]. We consider the systematic corrections of each clock with the exception of the lattice light shift to be fully correlated between all measurement campaigns. The lattice light shift is remeasured in each campaign and thus is only correlated within a campaign.

TABLE I. Typical contributions to the fractional systematic clock uncertainties of Sr1 and Sr2 in 10^{-18}. BBR stands for blackbody radiation. For typical frequency shifts related to the effects, the reader is referred to Ref. [33] and Ref. [24] for Sr1 and Sr2, respectively. For Sr2, we differentiate between the two local (PTB I, PTB II) and the remote (MPQ) campaigns.

Uncertainty contribution	Sr1	Sr2		
		(PTB I)	(MPQ)	(PTB II)
Lattice light shift	3.0	8.3	19.8	35.5
BBR ambient	12.8	6.3	19.5	15.6
BBR oven	1.2	0	0	0
Second-order Zeeman	1.0	1.9	1.5	1.7
Cold collisions	0.4	7.6	11.8	0.9
Background gas	2.3	3.8	3.8	3.8
Servo error	0.1	0	2.2	0
Tunneling	6.8	0	0	0
dc Stark shift	0.7	<0.1	<0.1	<0.1
Probe light shift	<0.1	0.2	0.2	0.2
Line pulling	<0.1	<0.1	<0.1	<0.1
Total	15.1	13.6	30.5	39.0

Similarly, the redshift correction for each local campaign is fully correlated within each campaign. No further correlations are taken into account. For more information, see the Supplemental Material [38]. This results in a measured fractional local clock offset $\overline{\Delta\nu}_{loc}/\nu_0 = 50(32) \times 10^{-18}$, where the combined estimated measurement uncertainty largely arises from the systematic uncertainties of the two clocks. The fact that we observe a significant frequency offset between the clocks in the local comparisons is unexpected, because both clocks operate on the same transition $^1S_0$-$^3P_0$ of the same isotope ^{87}Sr. The reason for this remains unclear, even though detailed systematic investigations of the systematic frequency shifts have been performed. However, equal offsets have been observed before and after the transfer of Sr2 to MPQ (Figs. 2 and 3). It is therefore reasonable to assume that the offset during the remote clock comparison at MPQ had the same value as observed locally. Thus, we regard $\overline{\Delta\nu}_{loc}$ as a calibration for the clock's frequency ratio, as it is required if two clocks of different types with an unknown frequency ratio are used for chronometric leveling.

After the transportable clock was moved to MPQ, within one week ultracold ^{87}Sr atoms were trapped in the optical lattice and the clock transition was found. Optical frequency combs were placed at both ends for phase-coherent

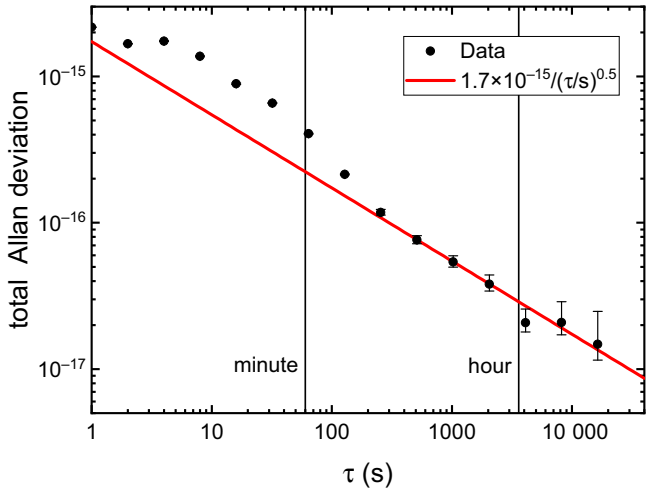


FIG. 4. Total Allan deviation of the concatenated data of the remote clock comparisons as a function of the averaging time τ. The red line indicates the instability and is a $\propto \tau^{-1/2}$ fit to points with $\tau > 200$ s.

frequency conversion [54,55] between the clock interrogation lasers at 698 nm and the 1542-nm laser that is used for frequency dissemination over the IFL.

Daily frequency offsets during the remote comparison are calculated in the same way as the local ones in Eq. (1), except for the to-be-inferred gravity potential term:

$$\Delta\nu^{\mathrm{rem}}_{\mathrm{day}} = \Delta\nu^{\mathrm{clock}}_{\mathrm{day}} + \mathrm{cor}^{\mathrm{Sr2}}_{\mathrm{day}} - \mathrm{cor}^{\mathrm{Sr1}}_{\mathrm{day}}. \tag{2}$$

The average remote clock offset $\overline{\Delta\nu}_{\mathrm{rem}}$ is again calculated as the weighted average of the daily ratios. Its uncertainty takes into account correlations of various systematic corrections as discussed above for the local comparisons. We find $\overline{\Delta\nu}_{\mathrm{rem}}/\nu_0 = 43\,645(36) \times 10^{-18}$. The daily frequency offsets of all three clock comparisons, two local and one remote, are shown in Fig. 3. The total Allan deviation, shown in Fig. 4, expresses the instability of the remote clock comparison. The IFL contribution only dominates the instability of the clock comparison data up to averaging times τ of about $\tau = 2$ s. To the best of our knowledge, this measurement constitutes the most stable transportable clock operation published so far. The instability is slightly higher in the remote clock comparison ($1.7 \times 10^{-15}/\sqrt{\tau/\mathrm{s}}$; Fig. 4) than in the local one ($1.0 \times 10^{-15}/\sqrt{\tau/\mathrm{s}}$; Fig. 2) as the transportable clock laser [56] was prestabilized to the ultrastable lasers at PTB [57,58] during the local comparisons.

Taking the local clock offset, $\overline{\Delta\nu}_{\mathrm{loc}}$, into account, the chronometrically measured geopotential difference $\Delta U_{\mathrm{chron}}$ between Sr2 at MPQ and Sr1 at PTB is then given by

$$\Delta U_{\mathrm{chron}} = \frac{c^2}{\nu_0}\left(\overline{\Delta\nu}_{\mathrm{rem}} - \overline{\Delta\nu}_{\mathrm{loc}}\right). \tag{3}$$

Its measured value is $3918.1(2.6)\,\mathrm{m^2 s^{-2}}$, which agrees with the independent, geodetic determination of $3915.88(0.30)\ \mathrm{m^2\ s^{-2}}$ (Fig. 3). The uncertainty of $\Delta U_{\mathrm{chron}}$ is determined by applying the methods described above to incorporate correlations.

The geodetic potential difference between reference points at PTB [59] and at MPQ [60] is computed by the GNSS/geoid approach, which is expected to be more accurate than geometric leveling for large distances, as it is not affected by systematic leveling errors.

The ellipsoidal height h from GNSS and the quasi-geoid height ζ are employed to derive the (physically defined) normal height as $H^N = h - \zeta$, which is then converted to a corresponding geopotential value [23]. The (quasi)geoid model EGG2015 [23] is utilized for this purpose. The model is based on the remove-compute-restore technique and combines a global long-wavelength spherical-harmonic model from the GOCE mission with high-resolution terrestrial gravity and terrain data. The EGG2015 model also includes several gravimetric densification surveys around metrological institutes in Europe, including the PTB and MPQ sites. Furthermore, error estimates including covariances are available in Ref. [23]. The GNSS/geoid approach is first used for the computation of the potential difference between the benchmarks near the clock experiments, while the remaining, small height differences between the benchmarks and the clocks are measured by geometric leveling and then converted to a potential difference using $g_{\mathrm{MPQ}} \approx 9.808\ \mathrm{m\ s^{-2}}$ and the value at PTB given above, respectively.

The given uncertainty of $0.30\ \mathrm{m^2\ s^{-2}}$ for the geopotential difference is based on the uncertainties (in height) of GNSS positioning (1.0 cm) and the EGG2015 model (1.9 cm), with negligible correlations. Furthermore, it should be noted that existing geometric leveling data from the German height network (DHHN92) have also been used to derive the potential difference between the PTB and MPQ clock positions, resulting in a deviation to the recommended value from the GNSS/geoid approach of only $0.3\ \mathrm{m^2\ s^{-2}}$ [23].

The previously discussed static but spatially variable components of the Earth's gravity field are the main contributions to the geopotential difference, while time-variable effects (mainly due to solid Earth and ocean tides) are below $0.5\ \mathrm{m^2\ s^{-2}}$ (maximum amplitude) for the potential difference between PTB and MPQ. Furthermore, the time-variable components largely average out over longer recording times and are thus neglected in this analysis. The total corresponding height uncertainties are 27 cm for the chronometric value and 3 cm for the geodetic value.

As shown in Fig. 4, we achieve a height resolution below 30 cm and a corresponding fractional frequency resolution of 3×10^{-17} within one hour of measurement, and 6 cm within one day. The instability is limited by the transportable clock Sr2, whereas that of Sr1 is about an order

of magnitude lower [33]. The main contribution is Dick noise [61] of the transportable clock laser [56]. Lower transportable clock instabilities can be realized in the near future, for example by using more stable transportable clock lasers [62] or by prestabilization methods [63].

In conclusion, we have demonstrated chronometric leveling over a distance of 457 km using a transportable lattice clock, a stationary clock as reference, and an IFL for frequency comparison. The chronometrically measured geopotential difference is determined with an uncertainty of 2.6 $m^2\ s^{-2}$, corresponding to a height uncertainty of 27 cm. Further studies will aim to reduce the systematic uncertainty of the transportable clock to the 10^{-18} level or below and to reduce its instability and thus the required averaging times. This will bring centimeter-level chronometric leveling within reach and could resolve existing discrepancies (at the centimeter to decimeter level) between the established geodetic methods, overcome their limitations, improve continental and global height reference frames, connect island and mainland height systems, connect tide gauges for sea-level monitoring, and contribute to gravity field modeling in combination with GNSS positions [13]. As an additional benefit, temporal variations of the gravitational field on a daily basis will be observable that are currently out of reach for other methods [64–66].

Acknowledgments. We thank Thomas Legero and Uwe Sterr for providing a stable laser oscillator and Andreas Koczwara for the development of electronics for the IFL. We acknowledge support by the Deutsche Forschungsgemeinschaft (DFG, German Research Foundation) under Germany's Excellence Strategy—EXC-2123 QuantumFrontiers—Project-ID 3908379.67, SFB 1464 TerraQ—Project-ID 434617780—within projects A04 and A05, and SFB 1128 geoQ within projects A03 and A04. This work was partially supported by the Max Planck-RIKEN-PTB Center for Time, Constants and Fundamental Symmetries.

[1] I. Ushijima *et al.*, Cryogenic optical lattice clocks, Nat. Photonics **9**, 185 (2015).
[2] N. Huntemann *et al.*, Single-ion atomic clock with 3×10^{-18} systematic uncertainty, Phys. Rev. Lett. **116**, 063001 (2016).
[3] K. Beloy *et al.*, Frequency ratio measurements at 18-digit accuracy using an optical clock network, Nature **591**, 564 (2021).
[4] Y. Huang *et al.*, Liquid-nitrogen-cooled Ca^+ optical clock with systematic uncertainty of 3×10^{-18}, Phys. Rev. Appl. **17**, 034041 (2022).
[5] K. Predehl *et al.*, A 920-kilometer optical fiber link for frequency metrology at the 19th decimal place, Science **336**, 441 (2012).
[6] C. Lisdat *et al.*, A clock network for geodesy and fundamental science, Nat. Commun. **7**, 12443 (2016).
[7] E. Cantin *et al.*, An accurate and robust metrological network for coherent optical frequency dissemination, New J. Phys. **23**, 053027 (2021).
[8] C. Clivati *et al.*, Common-clock very long baseline interferometry using a coherent optical fiber link, Optica **7**, 1031 (2020).
[9] T. Akatsuka *et al.*, Optical frequency distribution using laser repeater stations with planar lightwave circuits, Opt. Express **28**, 9186 (2020).
[10] M. Schioppo *et al.*, Comparing ultrastable lasers at 7×10^{-17} fractional frequency instability through a 2220 km optical fibre network, Nat. Commun. **13**, 212 (2022).
[11] M. Vermeer, *Chronometric Levelling*, Reports of the Finnish Geodetic Institute No. 83:2 (Geodeettinen Laitos, Geodetiska Institutet, Helsinki, Finland, 1983).
[12] A. Bjerhammar, On a relativistic geodesy, Bull. Géodésique **59**, 207 (1985).
[13] T. Mehlstäubler *et al.*, Atomic clocks for geodesy, Rep. Prog. Phys. **81**, 064401 (2018).
[14] C. W. Chou *et al.*, Optical clocks and relativity, Science **329**, 1630 (2010).
[15] M. Takamoto *et al.*, Test of general relativity by a pair of transportable optical lattice clocks, Nat. Photonics **14**, 411 (2020).
[16] Y. Huang *et al.*, Geopotential measurement with a robust, transportable Ca^+ optical clock, Phys. Rev. A **102**, 050802(R) (2020).
[17] D.-X. Liu *et al.*, Laboratory demonstration of geopotential measurement using transportable optical clocks, Chin. Phys. B **32**, 010601 (2023).
[18] T. Bothwell, Resolving the gravitational redshift across a millimetre-scale atomic sample, Nature **602**, 420 (2022).
[19] X. Zheng *et al.*, A lab-based test of the gravitational redshift with a miniature clock network, Nat. Commun. **14**, 4886 (2023).
[20] T. Takano *et al.*, Geopotential measurements with synchronously linked optical lattice clocks, Nat. Photonics **10**, 662 (2016).
[21] J. Grotti *et al.*, Geodesy and metrology with a transportable optical clock, Nat. Phys. **14**, 437 (2018).
[22] L. Sánchez *et al.*, Strategy for the realisation of the international height reference system (IHRS), J. Geod. **95**, 33 (2021).
[23] H. Denker *et al.*, Geodetic methods to determine the relativistic redshift at the level of 10^{-18} in the context of international timescales: A review and practical results, J. Geod. **5**, 487 (2018).
[24] S. B. Koller *et al.*, Transportable optical lattice clock with 7×10^{-17} uncertainty, Phys. Rev. Lett. **118**, 073601 (2017).
[25] S. Origlia *et al.*, Towards an optical clock for space: Compact, high-performance optical lattice clock based on bosonic atoms, Phys. Rev. A **98**, 053443 (2018).
[26] M. Gellesch *et al.*, Transportable optical atomic clocks for use in out-of-the-lab environments, Adv. Opt. Technol. **9**, 313 (2020).
[27] N. Ohmae *et al.*, Transportable strontium optical lattice clocks operated outside laboratory at the level of 10^{-18} uncertainty, Adv. Quantum Technol. **4**, 2100015 (2021).
[28] R. J. Fasano, A Transportable Ytterbium Optical Lattice Clock, Ph.D. thesis, University of Colorado, 2021.

[29] J. Stuhler *et al.*, Opticlock: Transportable and easy-to-operate optical single-ion clock, Measurement: Sensors **18**, 100264 (2021).

[30] F. Guo *et al.*, A proof-of-concept model of compact and high-performance ^{87}Sr optical lattice clock for space, AIP Adv. **11**, 125116 (2021).

[31] M. Zeng *et al.*, Toward a transportable Ca^{+} optical clock with a systematic uncertainty of 4.8×10^{-18}, Phys. Rev. Appl. **19**, 064004 (2023).

[32] S. Falke *et al.*, A strontium lattice clock with 3×10^{-17} inaccuracy and its frequency, New J. Phys. **16**, 073023 (2014).

[33] R. Schwarz *et al.*, Long term measurement of the ^{87}Sr clock frequency at the limit of primary Cs clocks, Phys. Rev. Res. **2**, 033242 (2020).

[34] S. M. F. Raupach *et al.*, Brillouin amplification supports 1×10^{-20} accuracy in optical frequency transfer over 1400 km of underground fibre, Phys. Rev. A **92**, 021801(R) (2015).

[35] G. Kramer and W. Klische, in *Proceedings of the 18th European Frequency and Time Forum, Guildford, UK* (IET, London, UK, 2004), p. 595.

[36] E. Benkler *et al.*, On the relation between uncertainties of weighted frequency averages and the various types of Allan deviations, Metrologia **52**, 565 (2015).

[37] I. Ushijima *et al.*, Operational magic intensity for Sr optical lattice clocks, Phys. Rev. Lett. **121**, 263202 (2018).

[38] See Supplemental Material at http://link.aps.org/supplemental/10.1103/PhysRevApplied.21.L061001 for additional information on the consideration of correlations in weighted averaging and the evaluation of systematic frequency shifts in the transportable clock.

[39] GUM, Evaluation of measurement data – guide to the expression of uncertainty in measurement, JCGM 100:2008 (2008).

[40] T. Middelmann *et al.*, High accuracy correction of blackbody radiation shift in an optical lattice clock, Phys. Rev. Lett. **109**, 263004 (2012).

[41] T. L. Nicholson *et al.*, Systematic evaluation of an atomic clock at 2×10^{-18} total uncertainty, Nat. Commun. **6**, 6896 (2015).

[42] C. Lisdat *et al.*, Blackbody radiation shift in strontium lattice clocks revisited, Phys. Rev. Res. **3**, L042036 (2021).

[43] A. Al-Masoudi *et al.*, Noise and instability of an optical lattice clock, Phys. Rev. A **92**, 063814 (2015).

[44] M. M. Boyd *et al.*, Nuclear spin effects in optical lattice clocks, Phys. Rev. A **76**, 022510 (2007).

[45] S. Dörscher *et al.*, Lattice-induced photon scattering in an optical lattice clock, Phys. Rev. A **97**, 063419 (2018).

[46] J. A. Muniz *et al.*, Cavity-QED measurements of the ^{87}Sr millihertz optical clock transition and determination of its natural linewidth, Phys. Rev. Res. **3**, 023152 (2021).

[47] X. Baillard *et al.*, Accuracy evaluation of an optical lattice clock with bosonic atoms, Opt. Lett. **32**, 1812 (2007).

[48] C. Shi *et al.*, Polarizabilities of the ^{87}Sr clock transition, Phys. Rev. A **92**, 012516 (2015).

[49] T. Bothwell *et al.*, JILA SrI optical lattice clock with uncertainty of 2.0×10^{-18}, Metrologia **56**, 065004 (2019).

[50] B. X. R. Alves *et al.*, in *2019 Joint Conference of the IEEE International Frequency Control Symposium and European Frequency and Time Forum (EFTF/IFC)* (IEEE, Orlando, FL, USA, 2019), p. 1.

[51] S. Falke, The ^{87}Sr optical frequency standard at PTB, Metrologia **48**, 399 (2011).

[52] P. Lemonde and P. Wolf, Optical lattice clock with atoms confined in a shallow trap, Phys. Rev. A **72**, 033409 (2005).

[53] R. Kacker *et al.*, Combined result and associated uncertainty from interlaboratory evaluations based on the ISO guide, Metrologia **39**, 279 (2002).

[54] E. Benkler *et al.*, End-to-end topology for fiber comb based optical frequency transfer at the 10^{-21} level, Opt. Express **27**, 36886 (2019), also see erratum [67].

[55] M. Giunta *et al.*, Real-time phase tracking for wide-band optical frequency measurements at the 20th decimal place, Nat. Photonics **14**, 44 (2020).

[56] S. Häfner *et al.*, Transportable interrogation laser system with an instability of mod $\sigma_y = 3 \times 10^{-16}$, Opt. Express **28**, 16407 (2020).

[57] S. Häfner *et al.*, 8×10^{-17} fractional laser frequency instability with a long room-temperature cavity, Opt. Lett. **40**, 2112 (2015).

[58] D. G. Matei *et al.*, 1.5 μm lasers with sub-10 mHz linewidth, Phys. Rev. Lett. **118**, 263202 (2017).

[59] F. Riedel, Direct comparisons of European primary and secondary frequency standards via satellite techniques, Metrologia **57**, 045005 (2020).

[60] H. Denker *et al.*, *Report on levelling and GNSS results for stations on the MPQ campus in Garching*, Tech. Rep. (2019).

[61] G. J. Dick, in *Proceedings of 19th Annu. Precise Time and Time Interval Meeting, Redendo Beach, 1987*, ADA502386 (U.S. Naval Observatory, Washington, DC, 1988), p. 133.

[62] S. Herbers *et al.*, Transportable clock laser system with an instability of 1.6×10^{-16}, Opt. Lett. **47**, 5441 (2022).

[63] H. Katori, Longitudinal Ramsey spectroscopy of atoms for continuous operation of optical clocks, Appl. Phys. Express **14**, 072006 (2021).

[64] C. Voigt *et al.*, Time-variable gravity potential components for optical clock comparisons and the definition of international time scales, Metrologia **53**, 1365 (2016).

[65] Y. Tanaka and H. Katori, Exploring potential applications of optical lattice clocks in a plate subduction zone, J. Geod. **95**, 1 (2021).

[66] M. Takamoto *et al.*, A perspective on the future of transportable optical lattice clocks, Appl. Phys. Lett. **120**, 140502 (2022).

[67] E. Benkler *et al.*, End-to-end topology for fiber comb based optical frequency transfer at the 10^{-21} level: erratum, Opt. Express **28**, 15023 (2020).